

---

# A hybrid approach to seismic deblending: when physics meets self-supervision

---

Nick Luiken, Matteo Ravasi, Claire E. Birnie

King Abdullah University of Science and Technology,

{nicolaas.luiken, matteo.ravasi, claire.birnie}@kaust.edu.sa

## Abstract

To limit the time, cost, and environmental impact associated with the acquisition of seismic data, in recent decades considerable effort has been put into so-called simultaneous shooting acquisitions, where seismic sources are fired at short time intervals between each other. As a consequence, waves originating from consecutive shots are entangled within the seismic recordings, yielding so-called blended data. For processing and imaging purposes, the data generated by each individual shot must be retrieved. This process, called deblending, is achieved by solving an inverse problem which is heavily underdetermined. Conventional approaches rely on transformations that render the blending noise into burst-like noise, whilst preserving the signal of interest. Compressed sensing type regularization is then applied, where sparsity in some domain is assumed for the signal of interest. The domain of choice depends on the geometry of the acquisition and the properties of seismic data within the chosen domain. In this work, we introduce a new concept that consists of embedding a self-supervised denoising network into the Plug-and-Play (PnP) framework. A novel network is introduced whose design extends the blind-spot network architecture of [28] for partially coherent noise (i.e., correlated in time). The network is then trained directly on the noisy input data at each step of the PnP algorithm. By leveraging both the underlying physics of the problem and the great denoising capabilities of our blind-spot network, the proposed algorithm is shown to outperform an industry-standard method whilst being comparable in terms of computational cost. Moreover, being independent on the acquisition geometry, our method can be easily applied to both marine and land data without any significant modification.

## 1 Introduction

Reflection seismology [40] is a geophysical technique that uses reflected seismic waves to characterize the Earth's subsurface. This method comprises of a controlled source of seismic energy and an array of receivers that record the pressure (or displacement) induced by the reflected waves. The physical instrumentation varies depending on the acquisition environment: for example, an airgun is used as seismic source in marine settings whilst a vibroseis is the preferred choice in land settings. Similarly, hydrophones (and possibly accelerometers) are towed behind a boat inside a so-called streamer cable or geophones (combined with hydrophones) can be laid directly on the seafloor for marine acquisition; whilst geophones are used for land acquisition. After the introduction of 3D seismic [11], today's conventional seismic acquisition campaigns may last several weeks up to a few months [7, 26, 10]. In an attempt to improve acquisition efficiency, and therefore limit the time, cost, and associated environmental impact, [6, 9, 3, 36] introduced a new paradigm in seismic acquisition usually referred to as *simultaneous shooting*. Simply put, consecutive sources are fired at short time intervals, thereby minimizing the overall acquisition time. This comes at the cost of recording entangled seismic data, also called *blended* data, where the waves originating from one source tend to

overlap with those originating from previous and subsequent sources. To render such data suitable for subsequent steps of seismic processing and imaging, the interference between consecutive shots must be removed such that the contribution of each individual source (also referred to as a *shot gather*) is retrieved. This process is called *deblending*. Mathematically speaking, blending is an operator that takes the otherwise conventionally acquired data and combines them together using a pre-defined sequence of time delays. In theory, deblending can be achieved by solving the associated inverse problem; however, as this problem is heavily underdetermined, choosing an appropriate regularization is fundamental to achieve a successful inversion. Historically, the design of suitable regularizers is motivated by the effect of the adjoint of the blending operator on the blended data. In fact, the resulting data can be seen as a superposition of coherent signal (i.e., reflections from the shot whose firing time has been properly accounted for) and trace-wise, burst-like noise (i.e., reflections from all other interfering shots whose firing times have not been properly accounted for).

The recent success of deep learning in various scientific disciplines has attracted the interest of the geophysical community, resulting in many opportunities and new challenges [50]. A common hurdle when applying deep learning methods to geophysical inverse problems is the lack of trustworthy training data. More specifically, whilst training data should consist of clean, representative ground truth examples that resemble the solution to the inverse problem at hand, such a solution generally does not exist a priori. Two approaches commonly adopted to circumvent this problem are to either generate synthetic data or to use state-of-the-art algorithms to produce input-output pairs to train a network on; in both cases, transfer learning [41, 34] or domain adaptation [2, 12] techniques are then required to generalize the network capabilities to unseen field data. A major drawback of this approach is that synthetic data may not resemble field data accurately enough to be considered a *representative* dataset: this is well-known in the geophysical community and has been a major criticism for decades when new methods are tested only on synthetic data. This also represents a serious roadblock to the application of deep learning methods in geophysics. Additionally, in most geophysical applications the underlying *physics*, or at least part of the physics, is well understood. Pure, end-to-end machine learning methods tend to ignore these well-studied physical principles, thereby discarding important a priori knowledge of the problem they are tasked to solve.

**Our contribution** We introduce a novel algorithm for seismic deblending, which blends the physics of the underlying physical process with a state-of-the-art self-supervised denoiser into a single, well-crafted inverse process. This is specifically achieved within the framework of Plug-and-Play (PnP) priors. Our network architecture is inspired by the blind-spot network of [28] and modified to handle trace-wise coherent noise. The network is trained on-the-fly at each PnP iteration in a self-supervised manner, completely bypassing the need for ground truth data. Our numerical experiments illustrate that the proposed algorithm can outperform a state-of-the-art conventional method. Finally, we show that our algorithm is independent on the underlying structure of the seismic data and can be used easily for different acquisition set-ups - a clear advantage over conventional methods.

## 2 Background

**The seismic data layout** Seismic data are commonly acquired by firing a source at a given time and recording the reflections arising from the interaction between the emitted seismic wave and changes in subsurface properties. Conceptually, seismic data can be arranged as a three dimensional tensor (or a cube), having the dimensions of the number of sources  $n_s$ , number of receivers  $n_r$ , and number of time samples  $n_t$ :  $d_c(x_s, x_r, t)$ . Slicing this cube in different directions give raise to so-called seismic gathers: more specifically, when slicing across the source axis, we obtain the data recorded by all receivers for a single shot, usually called a *Common Shot Gather* (CSG); conversely, by slicing across the receiver axis we obtain the data generated by all shots for a single receiver. When the receivers move alongside the source (i.e., marine case) the resulting gather is called the *Common Channel Gather* (CCG). For static receivers (i.e., ocean-bottom or land acquisition), the seismic gather is known as the *Common Receiver Gather* (CRG). Both scenarios will later be considered.

**Blended acquisition** In practice, to be able to collect data where no overlap exists between consecutive shots, each shot has to be fired with an appropriate time delay, such that all reflections from one shot have been recorded by the receivers before the next shot is fired. This dictates the overall acquisition time and greatly limits any possible acquisition speed-up. Alternatively, in blended acquisition, shots are fired at shorter intervals. This means that each individual CSG contains

recordings from both the nominal as well as the previous and subsequent shots. In this work, we consider the so-called *continuous blending* setting. This approach is state-of-the-art in marine seismic acquisition due to the fact it is easy to implement in the field. It is in fact simply achieved by firing the airgun towed by the acquisition vessel at short time intervals, and continuously recording the waves returning to the receiver array as depicted in figure 1. The recorded data  $d_b$  can be simply described as the superposition of all of the unblended, or clean, data shifted in time by the given time delay  $t_i = i \cdot T + \Delta t_i$ . Here,  $T$  is the nominal firing interval and  $\Delta t_i$  is a random dither applied to the nominal firing time of each shot. The blended data can thus be described as a function of the clean data

$$d_b = B d_c := [B_1, \dots, B_{n_s}] d_c = B_1 d_{c,1} + \dots + B_{n_s} d_{c,n_s} \quad (1)$$

where the blending operator is a horizontal stack of time-shift operators  $B_i$ , and the clean data is a vector where all vectorized shot gathers,  $d_{c,i} = \text{vec}(d_c(x_{s,i}, x_r, t))$ , are stacked together. Note that each  $B_i$  time-shift operator has the property that  $B_i^H B_i = I$ , and a composition of time-shift operators is again a time-shift operator.

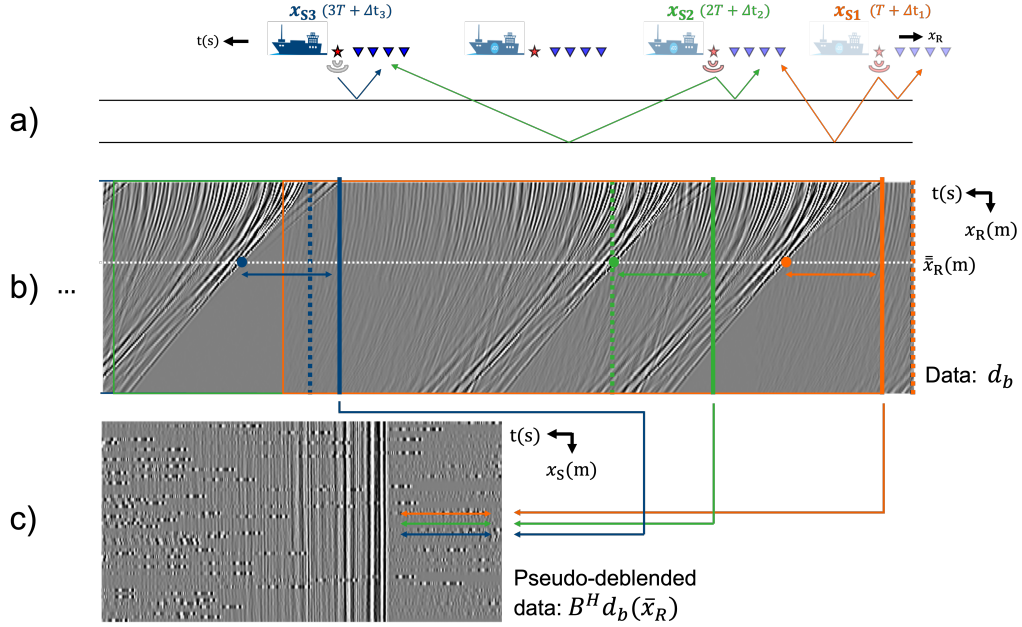


Figure 1: Schematic illustration of a seismic simultaneous shooting acquisition. a) Cartoon of a seismic acquisition campaign in continuous blending mode. A single vessel towing a source (red star) and an array of receivers (blue triangles) moves from right to left and fires energy into the ground at dithered periodic time samples. For each shot, reflections originated from shallow subsurface layers are immediately recorded by the receivers, whilst those produced by deeper reflectors are recorded later in time alongside the shallow reflections from the next firing shot. This phenomenon leads to the blending of independent shot gathers. b) A short time window of the continuously blended seismic data. Dashed vertical color lines represent the nominal firing times (i.e.,  $i \cdot T$ ), whilst the solid color lines represent the actual firing times with dithering. Color rectangles refer to every individual shot gather that we wish to separate from the other overlapping gathers. c) Pseudo-deblended data for a single receiver (white dashed line in panel b).

**Pseudo-deblending** To better understand how to design effective regularization strategies for the deblending problem, we first have to consider the action of  $B^H$  on the blended data. For the  $i^{th}$  shot gather, the result of  $B_i^H B d_c$  can be written as

$$\begin{aligned} & B_i^H (B_1 d_{c,1} + \dots + B_{n_s} d_{c,n_s}) \\ &= d_{c,i} + (B_i^H B_1 d_{c,1} + \dots + B_i^H B_{n_s} d_{c,n_s}) \end{aligned} \quad (2)$$

Therefore the action of  $B_i^H$  on the blended data produces the original  $i^{th}$  shot gather alongside randomly shifted versions of all the other shot gathers. Whilst these randomly shifted shot gathers are

coherent and look like standard seismic signal in the CSG domain, they appear as trace-wise coherent noise in the CRG (or CCG) domain as shown in the Experiments section. Because the application of the adjoint of the blending operator retrieves the true signal, albeit with some additional noise, its action is usually called *pseudo-deblending*. As a consequence of this, it is now clear that to retrieve the various  $d_{c,i}$ , an effective regularization must filter the trace-wise noise in CRGs (or CCGs) whilst preserving the coherent signal. Conventional approaches identify a domain in which the signal can be easily discriminated from the noise, and more specifically the signal in such domain is sparse whilst the noise is not. Examples of such a kind are the hyperbolic Radon transform for CRGs [25], the patched Fourier transform for CCGs [1], or the Curvelet transform [31]. It should be noted here that the performance and computational cost of such conventional approaches varies greatly. As explained later, a self-supervised denoiser can also be empowered to filter this noise, and, in fact, its denoising capabilities will be shown to be superior to those of commonly used, hand-crafted priors.

**Deblending by denoising** Deblending by denoising aims to deblend the data by directly denoising the pseudo-deblended CRGs. Deblending by denoising can be justified by noting that  $BB^H$  is a diagonal matrix. Therefore, making the substitution  $d_c = B^H z$  leads to

$$Bd_c = BB^H z = Dz,$$

where  $D$  is a diagonal matrix. The structure of  $D$  depends on the blending strategy. For continuous blending, the diagonal elements  $d_{ii}$  count the number of overlapping shots in each time-space sample of the blended data, which usually ranges from two to three. We can therefore approximate  $D = I$ , based on the argument that  $D$  is a simple amplitude correction. The solution is then given by

$$z = d_b \implies d_c = B^H d_b.$$

By doing so, the clean data,  $d_c$ , is approximated by the pseudo-deblended data,  $d_b$ , which however still contains the blending noise. Therefore, we can solve the following denoising problem to fully deblend the data:

$$\min_{d_c} \|d_c - B^H d_b\| + \mathcal{R}(d_c), \quad (3)$$

where  $\mathcal{R}(\cdot)$  is any chosen regularization. Because the distribution of the blending noise is far from being Gaussian, a typical choice for the data fidelity norm is  $\|\cdot\|_1$ . However, the  $\ell_1$ -norm in the data fidelity renders the solution non-trivial. Note that while in principle we could choose to denoise  $z$ , in this domain we do not have an appropriate regularization term, making it impossible to denoise.

**Deblending by inversion** Alternatively, one could retrieve the clean data by solving the (heavily) underdetermined inverse problem,

$$\min_{d_c} \frac{1}{2} \|Bd_c - d_b\|_2^2 + \mathcal{R}(d_c). \quad (4)$$

As the incoherent noise is fully explained by the blending operator, the  $\ell_2$ -norm for the data fidelity is an appropriate choice. From the above equation, it is not obvious how the noise appears in the data since we are not dealing directly with the pseudo-deblended data. The noise is however introduced into the solution through the gradient of the data term,  $B^H(Bd_c - d_b)$ . In sparse inversion, the objective is minimized iteratively by thresholding the gradient at every iteration, which can be interpreted as a noise removal step. The literature has shown that deblending by inversion is superior in comparison to deblending by denoising in terms of the overall quality of reconstruction.

**Self-supervised denoising: Incoherent noise** Self-supervised denoising is a recently introduced concept in the deep learning literature. This family of methods are designed in such a way that noisy images can be used as both the input and label to train a neural network to act as a denoiser, thereby bypassing the need for clean data as labels. Noise2Noise represents the first such method not relying on ground truth labels [29]. The network is forced to infer the signal from pairs of noisy data. For applications where such pairs are unavailable, an alternative was proposed in the concurrent works of [27] and [5], who introduced Noise2Void and Noise2Self, respectively. In both cases, the same image is used as input and label: under the assumption that the noise is incoherent whilst the signal is coherent, the network can naturally learn to infer only the signal from its neighbouring pixels. This mechanism bears similarity to classical statistical denoisers such as non-local means [15] or BM3D [18], however it relies on a more flexible nonlinear mapping using learned convolutional filters. More

specifically, to denoise a particular pixel, [27] replace the pixel of the input image with a randomly selected neighbouring pixel. As this pre-processing step introduces randomness in the central pixel of the receptive field of the network, the network should not learn anything from it and naturally learns to infer the signal from its neighbours (since the noise is assumed to be incoherent). Rather than directly replacing the pixel of interest, [5] pre-process the input image with a blind-spot (or donut) convolutional filter, so that the network once again cannot rely on the central pixel to predict itself. A key limitation of both approaches lies in the fact that the self-supervised loss can be evaluated only at the pixels that have been corrupted, making the training of these denoisers relatively slow. An alternative approach to blind-spot networks was introduced by [28]. Instead of corrupting the middle pixel, their network is explicitly designed to have a receptive field with a hole in the middle. This is achieved by combining padding and cropping with a standard convolution layer (i.e., to create a causal filter) and by rotating the input image four times prior to feeding it through the network. After the rotated inputs have been fed through the network, they are rotated back, concatenated, and combined by a series of  $1 \times 1$  convolutions prior to evaluating the loss at every pixel of the output image. A schematic description of this network is depicted in figure 2a.

**Self-supervised denoising: Coherent noise** Both Noise2Void and Noise2Self operate under the assumption that the noise is independent and identically distributed. [14] shows that the denoising quality of Noise2Void is degraded when the noise is structured. This shortcoming of Noise2Void is solved by masking pixels along the direction of the noise: the authors dub their method Structured Noise2Void. For the seismic blending problem, the noise that we are interested to suppress is also structured: more specifically, the blending noise shows correlation along the time axis. We, therefore, extend here the efficient implementation of [28] to suppress structured noise in seismic data, by simply using the original and flipped (over the time axis) version of the image as input. This produces a network whose receptive field is masked over an entire time trace, see figure 2b. In the following, we will call this network StructBS.

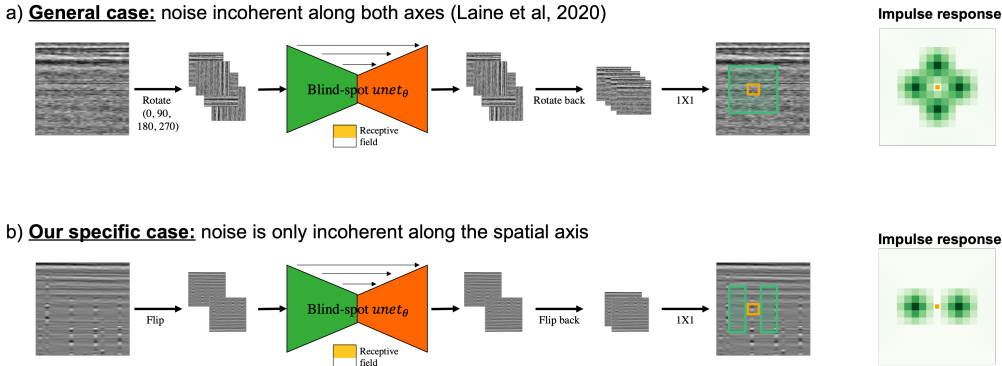


Figure 2: (a) The blind-spot network of [28], whose receptive field excludes the center pixel. (b) Our newly proposed blind-spot network, whose receptive field excludes an entire direction instead of just the middle pixel. Impulse responses are created by feeding the respective networks with unitary weights and zero biases with a image containing a unitary spike in the middle.

### 3 Related work

**Simultaneous shooting** Simultaneous shooting was first pioneered by [6] and has gained popularity in recent years [9]. Although the first attempts at deblending were mostly by means of denoising [33], recent research has revealed the superiority of deblending by inversion [1]. Since then, research has been devoted to finding appropriate regularization terms. Some approaches involve median-filtering [23, 22, 24], rank-reduction methods [17, 54], sparse regularization [30, 31, 55, 56, 58], and deep learning [42, 57, 48]. All the deep learning approaches to date use CNNs and require pre-training. [4] uses the RED framework introduced in [37], which is similar to the PnP framework. The difference is that RED explicitly incorporates the denoiser into the objective function. The authors propose the use of two conventional regularization techniques as a denoiser, the patched Fourier transform [1] and the singular-spectral-analysis filter [17], instead of applying them as a sparse penalty.

**Self-supervised seismic denoising** Seismic data are a prime example of a noisy data type where no clean, ground truth labels are available. As such, the application of self-supervised denoisers has recently been proposed for the suppression of different types of noise present in seismic data. Following the Noise2Void methodology, [13] use blind-spot networks for the suppression of random noise in post-stack seismic data. Expanding on this, [32] adapted the methodology of StructuredNoise2Void [14] for the suppression of trace-wise noise in seismic shot gathers, originating from poorly coupled receivers and/or dead sensors. The method that is most closely related to ours is the one presented in [48] - both with respect to application and methodology. The authors propose to use a self-supervised denoising network to deblend the data by denoising. To produce satisfactory results they require a number of additional pre- and post-processing steps. In our work, we incorporate a deep learning based denoiser in deblending by inversion, thereby leveraging both the underlying physics and the power of neural networks. Moreover, no pre- and post-processing is required.

**The Plug-and-Play framework** The Plug-and-Play framework was pioneered by [47]. The authors considered a number of popular denoisers, including BM3D [19], K-SVD [20], PLOW [16] and q-GGMRF [44]. In subsequent works, the denoisers have been replaced by pre-trained neural networks, most notably CNN and DnCNN. An extensive list of references is provided in [51], and include [37, 53, 35, 45, 21, 46, 30, 43, 52]. This research focuses mostly on properly training the neural networks such that they generalize well to different noise levels. The novelty of our method is that there is no pre-training with clean data required.

## 4 Method

Equipped with a self-supervised denoiser, a straightforward approach to deblending is to directly denoise the pseudo-deblended data. However, deblending by denoising is known to be sub-optimal in comparison to deblending by inversion. On the other hand, because a denoiser cannot be naturally added as a constraint to the objective function in equation 4, it is not immediately clear how to incorporate the denoiser into the inversion process.

**PnP derivation** The PnP framework is derived from the ADMM algorithm, which we will shortly derive here. The ADMM algorithm is generally used to solve inverse problems of the form

$$\min_x \mathcal{D}(\mathcal{M}(x), d) + \mathcal{R}(x),$$

where  $\mathcal{M}$  is the forward model,  $d$  is the measured data,  $\mathcal{D}$  is a data fidelity term that is generally smooth, and  $\mathcal{R}$  is a convex, possibly non-smooth regularization term. To account for the non-smoothness of  $\mathcal{R}$ , an auxiliary variable  $y = x$  is introduced, yielding the optimization problem

$$\min_{x,y} \mathcal{D}(\mathcal{M}(x), d) + \mathcal{R}(y) \text{ subject to } x = y.$$

The ADMM solves this problem by forming the so-called *augmented Lagrangian*,

$$\max_u \min_{x,y} \mathcal{D}(\mathcal{M}(x), d) + \mathcal{R}(y) + \frac{\rho}{2} \|x - y\|_2^2 + u^T(x - y),$$

where  $u$  is the Lagrange multiplier and  $\rho$  is a scalar. This problem is solved by alternatively minimizing over  $x$  and  $y$ , and maximizing over  $u$ . This yields the following scheme:

$$\begin{aligned} x_{k+1} &= \arg \min_x \left\{ \mathcal{D}(\mathcal{M}(x), d) + \frac{\rho}{2} \|x - y_k + u_k\|_2^2 \right\} \\ y_{k+1} &= \arg \min_y \left\{ \mathcal{R}(y) + \frac{\rho}{2} \|x_{k+1} - y + u_k\|_2^2 \right\} \\ u_{k+1} &= u_k + x_{k+1} - y_{k+1}. \end{aligned}$$

The key observation of [47] is that the  $y$ -update can be interpreted as a denoising inverse problem. As such, the authors propose to drop the user-defined regularization  $\mathcal{R}(\cdot)$  and instead plug in a denoiser of choice in the  $y$ -update of the ADMM iterations. Equipped with a powerful self-supervised denoiser that can filter the blending noise, we embed this into the PnP framework. Our proposed algorithm reads as follows:

$$\begin{aligned} x_{k+1} &= \arg \min_x \left\{ \frac{1}{2} \|Bx - d_b\|_2^2 + \frac{\rho}{2} \|x - y_k + u_k\|_2^2 \right\} \\ y_{k+1} &= \text{StructBS}_\theta(x_{k+1} + u_k) \\ u_{k+1} &= u_k + x_{k+1} - y_{k+1}. \end{aligned}$$

where  $x$  is used here for simplicity in place of  $d_c$ , and the  $x$ -update is solved by means of LSQR.

## 5 Experiments

In the following, our algorithm is tested on the openly available Mobil AVO viking graben line 12 marine dataset <sup>1</sup>. As the data has been originally acquired in a conventional fashion, we create the blending operator and blend the data ourselves. In addition to containing all the challenging features of a field dataset, this also provides us with a ground truth  $d_c$  onto which to assess the quality of our reconstruction. In this example, the original dataset is composed of  $n_s = 64$  sources,  $n_r = 120$  receivers, and  $n_t = 1024$  samples (i.e., the total recording time per shot equals 4 seconds). For the continuous blending operator, we choose a fixed firing interval of  $T = 2$  seconds, with added random delays selected uniformly in the interval  $\Delta t_i \sim [-1, 1]$  seconds. This overlap is quite challenging as generally half of the signal overlaps with either that of the previous or that of the next shot. Moreover, some pseudo-deblended shot gathers exhibit contributions from three consecutive shots. Finally, the relative mean-square error,  $RMSSE = \|d_c - d_{c,true}\|_2 / \|d_{c,true}\|_2$ , is chosen as a metric of comparison in all of our numerical examples. All experiments are performed on a Intel(R) Xeon(R) CPU @ 2.10GHz equipped with a single NVIDIA GeForce RTX 3090 GPU.

**Deblending by inversion with FISTA** To begin with, our newly proposed methodology is compared with the state-of-the-art deblending algorithm of [1] that solves the deblending problem as a sparsity promoting inversion

$$z_\star = \arg \min_z \|BFz - d_b\|_2^2 + \lambda \|z\|_1, \quad d_b = Fz_\star, \quad (5)$$

where  $F$  is a linear operator that performs a patched two-dimensional Fourier transform, and  $z_\star$  is the solution in the Fourier domain that is ultimately transformed back to the original time-space domain of the seismic data. In our experiment, the size and number of patches as well as the regularization parameter  $\lambda$  are selected by hand to yield optimal results. Moreover, the FISTA [8] solver is used with an adaptive decreasing sequence,  $\lambda_k$  (as this has been shown in the literature to outperform a fixed  $\lambda$  for this specific problem). We choose the sequence  $\lambda_k = \left(\frac{6}{5}e^{-0.05k} + 6\right) \lambda_0$ , which was once again fine-tuned to give the best performance. The final error is roughly 9.8%; hereon in this represents the benchmark against which we will assess the effectiveness of our self-supervised PnP algorithm.

**Deblending by inversion with PnP** Next, our PnP algorithm is applied to the same dataset. We choose 30 outer iterations, 3 inner iterations,  $\rho = 1$  and 30 denoiser epochs. The choice of these hyperparameters will be justified in the ablation study. We also use the U-Net architecture in [28] and the  $L_1$  norm for the self-supervised training loss because it is more appropriate for burst-like noise. Since the denoiser is trained on all the CCGs, the size of our training data is 120 and we use a batch size of 8. This leads to a solution that has an overall error of roughly 6.7%, which is approximately 3% lower than the conventional method. Figure 3a displays the relative error as function of the FISTA iterations. One of the patches into which the pseudo-deblended data has been decomposed alongside its Fourier spectrum are shown in figure 3d and 3b, respectively. The presence of burst-like noise translates into a non-sparse Fourier spectrum. On the other hand, the noise is removed in the deblending results in 3e as a result of a much sparser Fourier spectrum obtained during the inversion process as shown figure 3c. As a visual comparison, figure 4 displays the results for a given CCG (top) and CSG (bottom) for both the conventional and proposed approaches. It is noteworthy that our algorithm shows a clear improvement in terms of denoising capabilities, as visible in the displayed CCG. Especially after  $t = 2s$ , where the signal is weak and blending noise dominates, the conventional approach tends to be more prone to signal leakage compared to our PnP algorithm. Finally, the computational cost of the conventional algorithm can be quantified in terms of the number of forward and adjoint operations for both the blending ( $B$ ) and patched Fourier ( $F$ ) operators: in our example, this amounts to 200 forward and adjoint passes. On the other hand, our method requires 90 forward and adjoint passes for the blending operator and a total of 900 training epochs for the network. Considering that all computations (apart from the network related ones) are performed on the CPU, the two algorithms are comparable in terms of overall computational time (2h and 34mins for the conventional algorithm and 1h and 51mins for the PnP algorithm).

<sup>1</sup>[https://wiki.seg.org/wiki/Mobil\\_AVO\\_viking\\_graben\\_line\\_12](https://wiki.seg.org/wiki/Mobil_AVO_viking_graben_line_12)

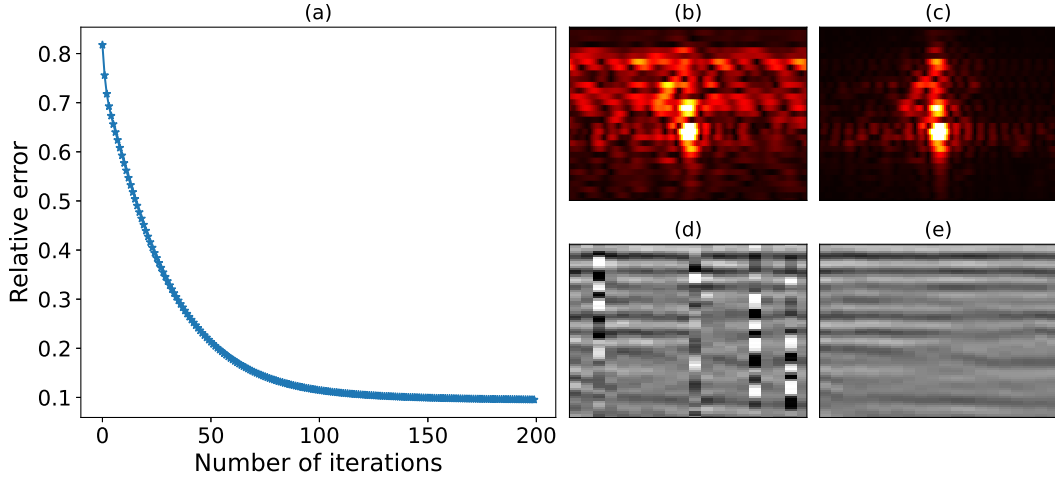


Figure 3: a) Error for the patched Fourier inversion. b) Extracted patch in the Fourier domain for the pseudo-deblended data. c) Extracted patch in the Fourier domain for the deblended data. d) Extracted patch of the pseudo-deblended data. e) Extracted patch of the deblended data.

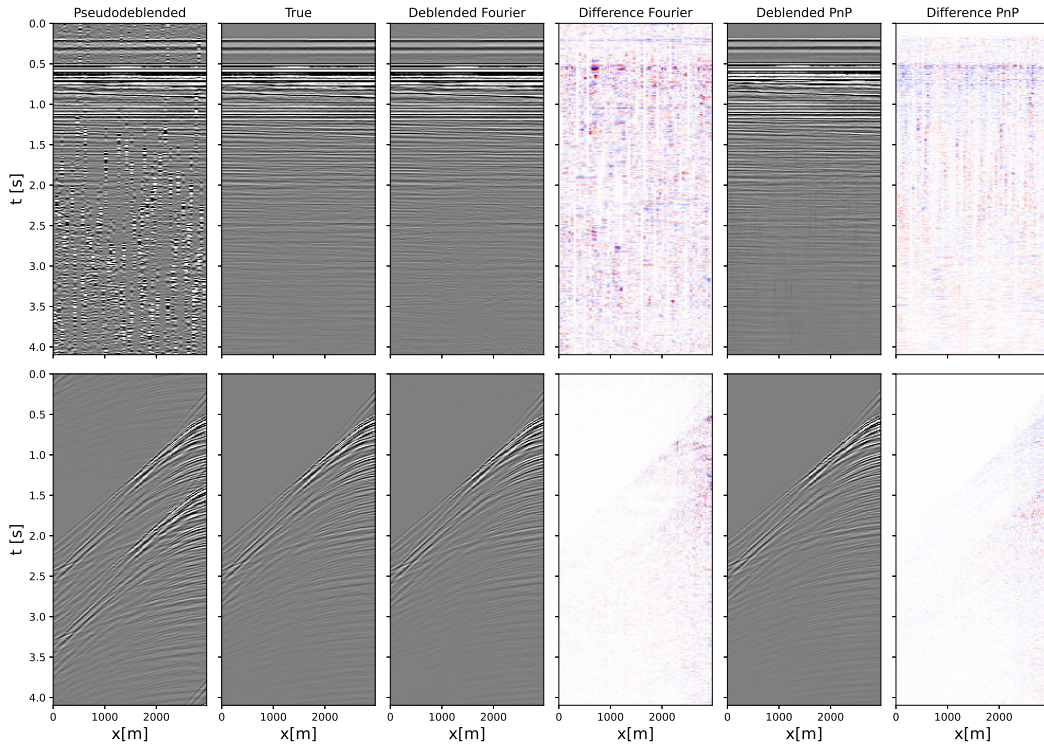


Figure 4: Deblending results for one CCG (top) and CSG (bottom). Although both algorithms can successfully remove most of the blending noise, our algorithm is less prone to signal leakage and provides better amplitude fidelity - a key factor in seismic data processing.

**PnP solution progression** To show how the solution progresses as a function of outer iterations, we select a receiver gather and show  $x_k$  in figure 5. We clearly see the noise level drop, which explains the need to keep training the network as shown in the paper. Lastly, we show a denoised receiver gather after every epoch of training, for outer iterations 1, 10, 20 and 30 in figures 12 13, 14 and 15 in the appendix.



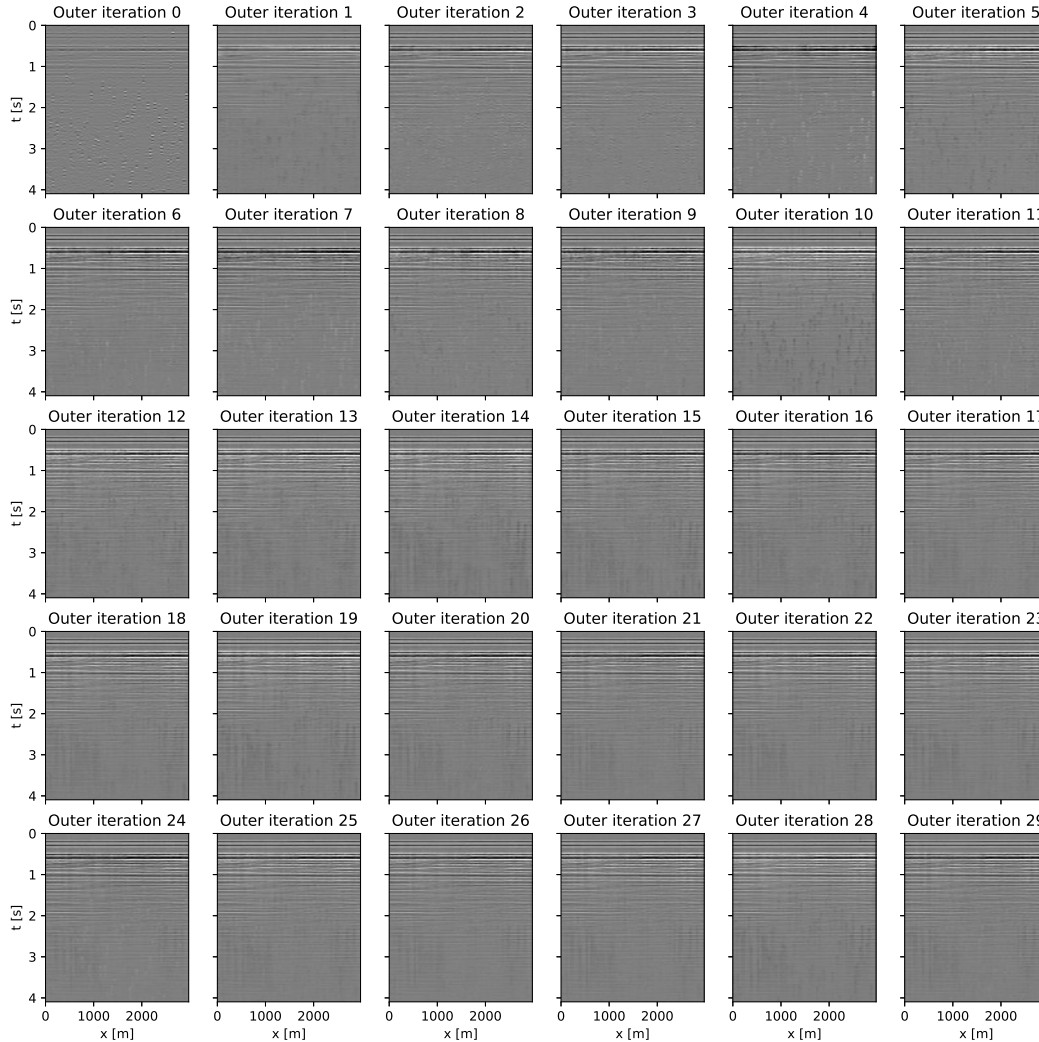


Figure 5: Progression of  $x_k$  for one receiver gather.

**PnP on ocean-bottom cable scenario** In this section we show that our algorithm generalizes well to other acquisition geometries. More specifically, we mimic here an ocean-bottom cable acquisition scenario where both CSGs and CRGs contain hyperbolic events. Despite the denoising process is here applied on data that presents a different structure when it comes to the coherent signal, our PnP algorithm is still very successful and achieves an overall error of 6.7%. We choose 3 inner iterations,  $\rho = 1$ , and 20 denoiser epochs and let the algorithm run for a total of 40 outer iterations. The reconstructions are shown in figure 6.

### 5.1 Ablation study

This section provides an extensive analysis of some of the key components of the proposed PnP methodology and their impact on the overall solution of the deblending inverse problem.

**PnP iterations** To begin with, we assess the importance of the PnP iterations compared to simply training the self-supervised denoiser on pseudo-deblended data and applying it directly to the entire dataset. Although not shown here, the result of this *one-shot denoising* produces a solution with an overall error of roughly 19%. This is much worse than both the conventional and PnP method and therefore considered not suitable.

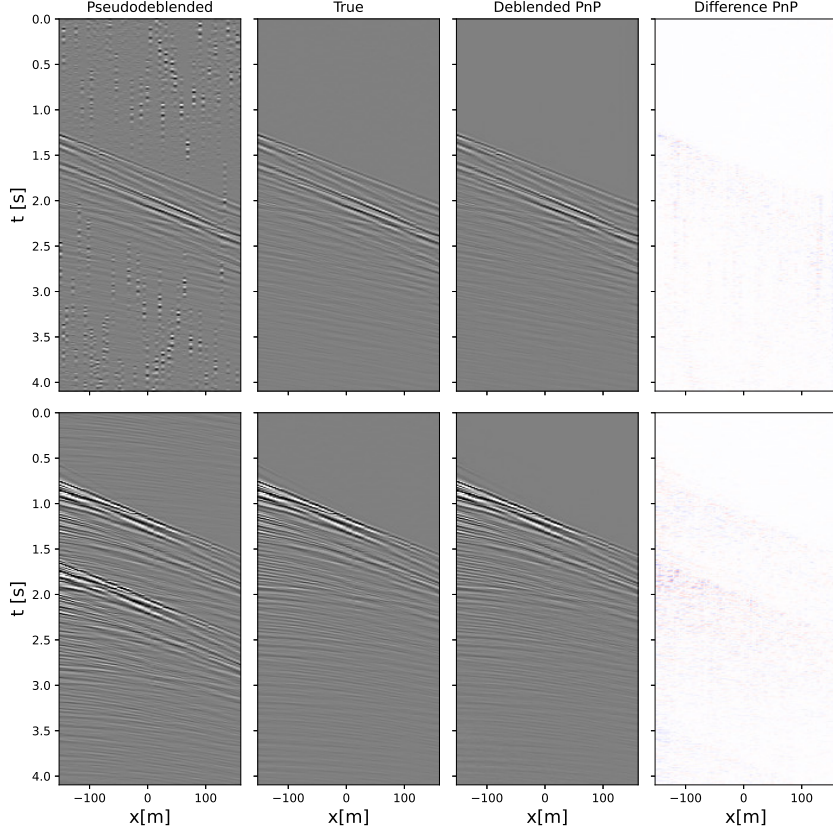


Figure 6: Deblending results for one CRG (top) and CSG (bottom) in ocean-bottom configuration.

**The  $x$ -update** As previously explained, the  $x$ -update requires the solution of the linear system

$$\min_x \frac{1}{2} \left\| \begin{bmatrix} B \\ \sqrt{\rho}I \end{bmatrix} x - \begin{bmatrix} d \\ \sqrt{\rho}(y_k - u_k) \end{bmatrix} \right\|_2^2, \quad (6)$$

which can be efficiently accomplished via LSQR. The convergence rate of LSQR depends on the spectrum of the blending operator  $B$ , specifically on its condition number [39, section 6.11.3]. As the singular values of  $B$  are the number of overlapping shots at each time step in the blended data, in our experiment the condition number is 3. Nevertheless, the number of inner iterations represents a hyperparameter that should be assessed. In order to do so,  $\rho$  and the number of epochs used to train the denoiser are fixed whilst the number of inner iterations for our PnP algorithm is varied between 1, 3, and 5. In all cases, the relative error as a function of outer iterations is computed and shown in figure 7a. As expected, increasing the number of inner iterations does not improve the overall solution. Somewhat surprisingly, the number of inner iterations exhibits a regularizing behaviour, in the sense that there seems to be an optimal number (here 3) above and below which the solution is poorer. When using fewer iterations, the overall error decreases slower in the first few outer iterations and quickly plateaus at around 20%. On the other hand, when using more iterations, the initial convergence is as fast as that of the optimal value, however the overall solution is of poorer quality. Another important hyperparameter is the augmented Lagrangian scalar  $\rho$ . For our algorithm,  $\rho$  takes the role of a regularization parameter that controls the discrepancy between  $x_{k+1}$  and  $y_k + u_k$ . We test three values,  $\rho = 0.1, 1$  and  $10$ , and choose the number of denoiser epochs that gives the lowest error. Again, we compare the relative error as a function of outer iterations (figure 7b). In the very first  $x$ -update,  $y_k$  and  $u_k$  are 0. Therefore, the linear system in equation 6 amounts to solving a Tikhonov regularized problem with regularization parameter  $\rho$ . For  $\rho = 10$ , the solution shrinks to values close to zero because  $\sigma_{\max}(B) \ll \rho$ . Therefore, to obtain a meaningful result, we set  $\rho = 0$  in the first outer iteration and then switch to  $\rho = 10$ . Nevertheless, looking at the error curve, it is clear that  $\rho = 10$  is too large: this is not unexpected because  $\sigma_{\max}(B) \ll \rho$  and the regularization terms dominates

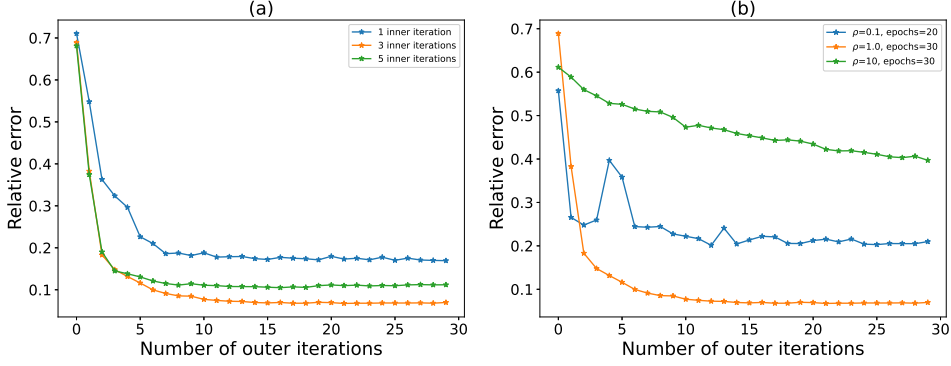


Figure 7: a) The error for fixed  $\rho$  and denoiser epochs as a function of the inner iterations. b) Error for fixed number of inner iterations and denoiser epochs and variable  $\rho$ .

the inversion at each outer step. Clearly,  $\rho = 1$  is the best choice, which is interesting because it is also the value that lies in the same order of magnitude of the singular values of  $B$ . This implies that there is a perfect balance between data misfit and regularization, which seems to be beneficial to the PnP algorithm. As stated before, the parameter  $\rho$  also controls the discrepancy between  $x$  and  $y$ . Theoretically, if the PnP algorithm were to converge,  $u \rightarrow u_*$  as  $k \rightarrow \infty$ , then  $x_k = y_k$  as  $k \rightarrow \infty$ . Therefore, the difference between  $x_k$  and  $y_k$  is a good measure of the convergence of the algorithm. Figure 8 shows the progression of  $x_k$  and  $y_k$  over the number of outer iterations. In the scenario where  $\rho$  is small,  $x_k$  and  $y_k$  are not close, indicating that the algorithm does not

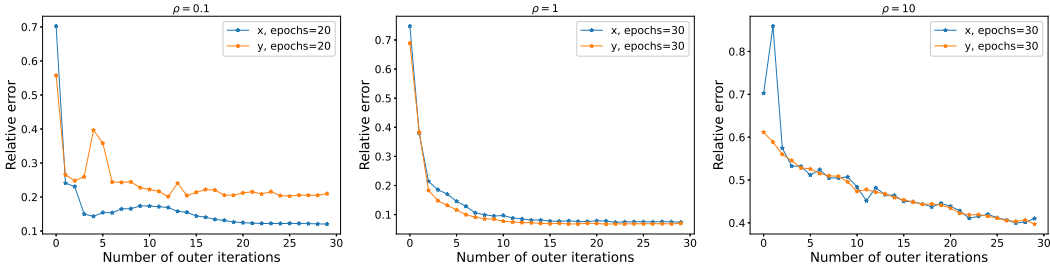


Figure 8: RMSE of  $x_k$  and  $y_k$  for different  $\rho$ .

converge. Interestingly,  $x_k$  has a lower error than its denoised counterpart  $y_k$ . On the other hand, the choice  $\rho = 10$  is clearly too large, which is to be expected from the fact that  $\sigma_{\max} = 3$ . In this case, whilst after a few iterations  $x_k$  and  $y_k$  become similar, the overall reconstruction error remains very high. For  $\rho = 1$ , the iterates  $x_k$  and  $y_k$  do seem to converge to a satisfactory solution. Although the blending operator depends on the firing times during acquisition, its sensitivity to  $\rho$  is dictated by its spectrum. Moreover, the noise level of the blending noise is likely to be similar for different blending scenarios: the noise will always be of the same order of magnitude as that of the signal. As the spectrum of different blending operators will also be similar, it seems safe to conclude that  $\rho = 1$  is a choice that is likely to work for our algorithm in general. Additionally, although not applied in our numerical examples, the difference between  $x_k$  and  $y_k$  would represent a good stopping criterion for our algorithm.

**The  $y$ -update** In our implementation we propose to start with a randomly initialized network and train it for a fixed number of epochs at every outer iteration. A warm start strategy is employed such that the weights of the network at a given outer iteration are initialized to those obtained at the end of the training of the previous outer iteration. The efficacy of this approach is shown in figure 9a, where we compare on-the-fly training with and without warm starts, where the latter re-initializes the network at every  $y$ -update. From the error curves, we can safely conclude that warm starting the network is clearly beneficial. Since there is no theoretical justification for this particular strategy, we consider a few other alternative strategies. The first strategy is to use a pre-trained network. Here pre-training is achieved by denoising the pseudo-deblended data in a self-supervised manner; this

approach could greatly reduce the computational cost of the overall algorithm since we do not need to train the network at every iteration. A comparison of the relative error with that of the proposed, on-the-fly training shown in figure 9b reveals that after a few outer iterations, the network is unable to further remove the remaining noise in the data. Another option is to stop training the network after a

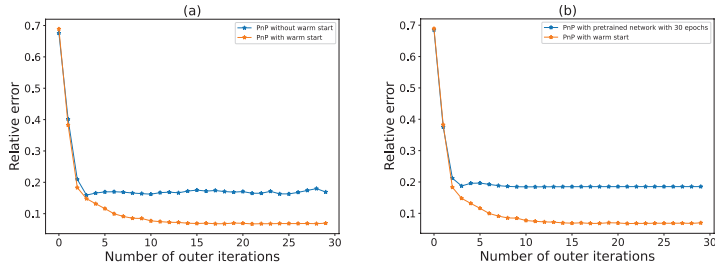


Figure 9: a) Error for network training with and without warm starts. b) Error when running the PnP algorithm with a network pre-trained on the pseudo-deblended data.

few outer iterations. Ideally, the network will have learnt how to remove the noise encountered during the first iterations, and extra training will not improve the denoiser capabilities. We run experiments where we stop the training after a fixed number of outer iterations to see whether there is an added benefit to continuing training the network. Results are shown in figure 10a. In all of the scenarios we

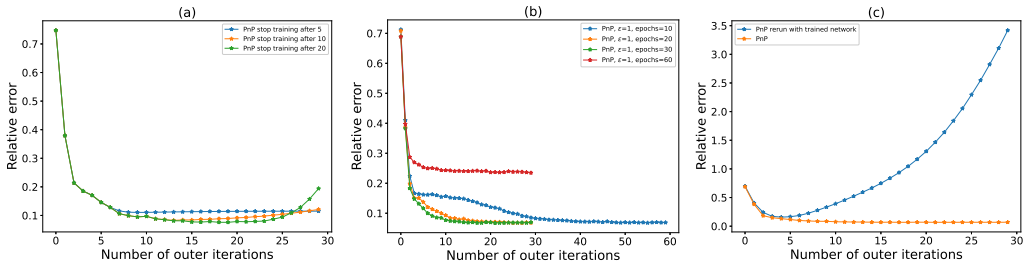


Figure 10: a) Error for on-the-fly training where training is stopped after a certain number of outer iterations. b) Error for different number of training epochs. c) Error when using the network at the end of the PnP algorithm for the entire process versus our proposed on-the-fly training strategy.

clearly see that stopping the training after a certain number of outer iterations leads to a stagnation in the error, or even worse to an increase in the error at later iterations. This behaviour is known as *semiconvergence* in the inverse problems community. Both results are perhaps not surprising, as the input to the network at every iteration contains a different noise level compared to that of earlier iterations: the noise in  $x_k$  constantly reduces during the overall inversion. Therefore, the network is required to learn a slightly different task at each time. In figure 10b, we assess the impact of the number training epochs for the denoiser. We clearly observe that at some point the curves for 30 and 20 epochs start to coincide, meaning that there is no additional gain in the extra 10 epochs of training. The curve for training with 10 epochs seems stagnant after the first three iterations, but eventually it picks up momentum and goes down again. Note that, in terms of overall epochs, the cost of performing 30 outer iterations with 10 epochs each is the same as using 10 outer iterations with 30 epochs each. However, every outer iteration carries an additional cost of three inner iterations for the  $x$ -update, which is not negligible as it requires evaluating the forward and adjoint of the blending operator. In general, it seems beneficial to perform more epochs in the early outer iterations, although there is a limit after which the error starts to stagnate. Moreover, training with 60 epochs leads to overfitting.

To further investigate the generalization capabilities of the network for blending problems, the network weights are saved after the last outer iteration of the PnP algorithm. The PnP algorithm is then re-run using the saved network without performing any on-the-fly training. Figure 10c shows that this strategy fails, illustrating that the network may have forgotten how to deal with the higher noise levels encountered in the early iterations. This results highlights the importance of using a self-supervised denoiser that can be easily and cheaply trained on-the-fly. The use of pre-trained denoising networks such as DnCNN may instead require training multiple networks with different

noise levels, unless a bias-free, non-blind network is used [51].

Finally, in order to assess the influence of network initialization on the final deblending results, we run our algorithm for 10 different random initializations of the network weights and biases. We show the resulting error curves as function of outer iterations in figure 11a. Moreover, figure 11b displays a box plot of the final relative errors compared to that of the conventional patched Fourier approach. We can observe that apart from one seed, all the others tend to produce a final deblending result of superior quality to the benchmark algorithm.

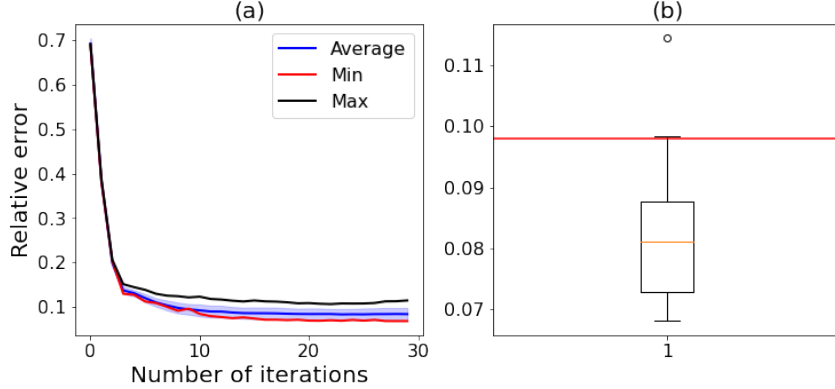


Figure 11: a) The average relative error plus and minus one standard deviation as function of outer iterations. Min and max error curves are also displayed based on the error after 30 iterations. b) Box plot of the relative error after 30 outer iterations for 10 different seeds. A horizontal red line indicates the error by the conventional patched Fourier approach.

## 6 Limitations and Conclusions

**Limitations** Our algorithm requires the setting of a number of hyperparameters, namely the number of inner and outer iterations, the parameter  $\rho$ , and the number of epochs for the self-supervised denoiser. The number of epochs seems to have a major impact on the quality of the deblending process and the overall convergence properties of our algorithm. Perhaps an adaptive strategy may reduce the computational cost without impacting the quality of the reconstruction. Since we warm start each training process, one could hypothesize that some of the shallow features learned at one iteration may be still valid for the subsequent denoising task. Moreover, additional hyperparameters that have not been explored in this work are associated with the network itself, e.g. the number of layers, the activation function, batch size, etc. This is also a direction for further research. Another possible drawback of our approach is the lack of convergence guarantees. PnP methods have been shown to converge under certain assumptions, one of them being that the physical operator in the data misfit term, in our case the blending matrix  $B$ , has to be strongly convex [38]. This requirement is never met for the deblending problem, as  $B$  is always underdetermined. Empirically, we observe that  $x_k$  and  $y_k$  tend to converge to similar values for some carefully selected hyperparameters, indicating that at least in our experiments the algorithm converges successfully. Moreover, the distance between  $x_k$  and  $y_k$  may be used as a suitable stopping criterion for the outer iterations, which is another hyperparameter that is currently set upfront. Similarly, to obtain convergence guarantees for the PnP method, the denoiser has to be Lipschitz continuous; when a neural network is used, this means that spectral normalization is required during training. In [49], it was shown that PnP algorithms can be convergent when combined with carefully pre-trained denoisers that satisfy such condition.

**Societal impact** Blended acquisition greatly reduces the time required to acquire seismic data, thereby limiting the impact of seismic acquisitions on the environment. Apart from shooting at shorter intervals, there is no difference compared to conventional acquisition. Moreover, since a larger number of shots can be fired in the same overall acquisition time, recent research has suggested that the energy emitted by each source could be lowered. This may provide acquisition solutions that are more environmentally friendly for marine life.

**Conclusions** We have introduced a novel hybrid algorithm for seismic deblending, combining the physics of the blending operator with a self-supervised denoiser that is naturally embedded into the Plug-and-Play framework. We have adapted the network architecture in [28] to enforce an extended blind spot along an entire axis (time, in our case) instead of single pixels. Because the denoiser is self-supervised, our approach bypasses the need for ground truth labels that are usually unavailable for seismic applications. Experiments on a field dataset have shown that the proposed method can outperform a state-of-the-art, sparsity-based algorithm. Moreover, our algorithm is independent on the type of acquisition, which is usually an issue for conventional algorithms. Although our algorithm requires the setting of a number of hyperparameters, we have argued that the number of inner iterations and  $\rho$  can most likely be set to a fixed number and this easily generalizes to different seismic acquisitions. However, the network architecture and the number of epochs may require tuning for different acquisition setups. We hope to address these issues by having an adaptive strategy for setting the number epochs in future work.

## References

- [1] R. Abma, D. Howe, M. Foster, I. Ahmed, M. Tanis, Q. Zhang, A. Arogunmati, and G. Alexander. Independent simultaneous source acquisition and processing. *Geophysics*, 80(6):WD37–WD44, 2015.
- [2] T. Alkhalifah, H. Wang, and O. Ovcharenko. Mlreal: Bridging the gap between training on synthetic data and real data applications in machine learning. *arXiv*, 2021.
- [3] C. Bagaini. Acquisition and processing of simultaneous vibroseis data. *Geophysical Prospecting*, 58:81–99, 2010.
- [4] B. Bahia, R. Rongzhi Lin, and M. Sacchi. Regularization by denoising for simultaneous source separation. *Geophysics*, 86(6):1942–2156, 2021.
- [5] J. Batson and L. Royer. Noise2self: Blind denoising by self-supervision. *International Conference on Machine Learning*, pages 524–533, 2019.
- [6] C.J. Beasley, R.E. Chambers, and Z. Jiang. A new look at simultaneous sources. In *68th Meeting, SEG Expanded Abstracts*, volume 2022, pages 133–135. European Association of Geoscientists & Engineers, 1998.
- [7] G. Beaudoin and A.A. Ross. Field design and operation of a novel deepwater, wide-azimuth node seismic survey. *The Leading Edge*, 26:385–544, 2007.
- [8] A. Beck and M. Teboulle. A fast iterative shrinkage-thresholding algorithm for linear inverse problems. *SIAM Journal on Imaging Sciences*, 2:183–202, 2009.
- [9] A. J. G. Berkhout. Changing the mindset in seismic data acquisition. *The Leading Edge*, 27:924–938, 2008.
- [10] M. Berraki, S. Buizard, J. Ramirez, R.M. Elde, D. Eckert S.S. Roy, and J.-F. Synnevag. Grane prm - from acquisition to interpretation in record time. In *79th EAGE Conference and Exhibition 2022*, volume 2017, pages 1–5. European Association of Geoscientists & Engineers, 2017.
- [11] B. Biondi. *3D Seismic Imaging Seismology (2nd ed.)*. SEG Books, 2006.
- [12] C. Birnie and T. Alkhalifah. Leveraging domain adaptation for efficient seismic denoising. In *Energy in Data Conference, Austin, Texas, 20–23 February 2022*, pages 11–15. Energy in Data, 2022.
- [13] C. Birnie, M. Ravasi, L. Sixiu, and T. Alkhalifah. The potential of self-supervised networks for random noise suppression in seismic data. *Artificial Intelligence in Geosciences*, 2:47–59, 2021.
- [14] C. Broaddus, A. Krull, M. Weigert, U. Schmidt, and G. Myers. Removing structured noise with self-supervised blind-spot networks. *2020 IEEE 17th International Symposium on Biomedical Imaging (ISBI)*, pages 159–163, 2020.
- [15] A. Buades, B. Coll, and J.-M. Morel. A non-local algorithm for image denoising. *IEEE Conference on Computer Vision and Pattern Recognition*, 2:60–65, 2005.
- [16] P. Chatterjee and P. Milanfar. Patch-based near-optimal image denoising. *Image Processing, IEEE Transactions on*, 21(4):161–175, 2012.
- [17] J. Cheng and M.D. Sacchi. Separation and reconstruction of simultaneous source data via iterative rank reduction. *Geophysics*, 80(4):V57–V66, 2015.
- [18] K. Dabov, A. Foi, V. Katkovnik, and K. Egiazarian. Image denoising by sparse 3-d transform-domain collaborative filtering. *IEEE Transactions on Image Processing*, 16:2080–2095, 2007.
- [19] K. Dabov, A. Foi, V. Katkovnik, and K. Egiazarian. Image denoising by sparse 3-d transform-domain collaborative filtering. *IEEE Transactions on image processing*, 16(8):2080–2095, 2007.
- [20] N. Elad and M. Aharon. Image denoising via sparse and redundant representations over learned dictionaries. *Image Processing, IEEE Transactions on*, 15(12):3726–3745, 2006.
- [21] S. Gu, R. Timofte, and L. van Gool. Integrating local and non-local denoiser priors for image restoration. In *International Conference on Pattern Recognition*, pages 2923–2928, 2018.
- [22] W. Huang, R. Wang, X. Gong, and Y. Chen. Iterative deblending of simultaneous-source seismic data with structuring median constraint. *IEEE Geoscience and Remote Sensing Letters*, 15(1):58–62, 2017.

- [23] S. Huo, Y. Luo, and P.G. Kelamis. Simultaneous sources separation via multidirectional vector-median filtering. *Geophysics*, 77(4):123–131, 2012.
- [24] S. Huo, Y. Luo, and P.G. Kelamis. Deblending using a space-varying median filter. *Exploration Geophysics*, 46(4):332–341, 2015.
- [25] A. Ibrahim and M.D. Sacchi. Simultaneous source separation using a robust radon transform. *Geophysics*, 79:V1–V11, 2014.
- [26] P.R.S. Johann, E.A. Thedy, F.A. Gomes, and M.C. Schinelli. 4d seismic in brazil: Experiences in reservoir monitoring. Offshore Technology Conference, 2006.
- [27] A. Krull, T.-O. Buchholz, and F. Jug. Noise2void - learning denoising from single noisy images. *Proc. IEEE Conf. Comput. Vision Pattern Recognit.*, 2019.
- [28] S. Laine, T. Karras, J. Lehtinen, and T. Aila. High-quality self-supervised deep image denoising. *Advances in Neural Information Processing Systems*, pages 6970–6980, 2019.
- [29] J. Lehtinen, J. Munkberg, J. Hasselgren, S. Laine, T. Karras, M. Aittala, and T. Aila. Noise2noise: Learning image restoration without clean data. *International Conference on Machine Learning (ICML)*, 2019.
- [30] C. Li, C.C. Mosher, and Y. Ji. An amplitude-preserving deblending approach for simultaneous sources. *Geophysics*, 84(3):V185–V196, 2019.
- [31] C. Li, C.C. Mosher, and Y. Ji. Randomized marine acquisition with compressive sampling matrices. *Geophysical Prospecting*, 60(3):648–662, 2019.
- [32] S. Liu, C. Birmie, and T. Alkhalifah. Coherent noise suppression via a self-supervised deep learning scheme. In *83rd EAGE Conference and Exhibition 2022*, volume 2022, pages 1–5. European Association of Geoscientists & Engineers, 2022.
- [33] A. Mahdad, P. Doulgeris, and G. Blacquiere. Separation of blended data by iterative estimation and subtraction of blending interference noise. *Geophysics*, 76:Q9–Q17.
- [34] S. Mandelli, V. Lipari, P. Bestagini, and S. Tubaro. Interpolation and denoising of seismic data using convolutional neural networks. *arXiv*, 2019.
- [35] T. Meinhardt, M. Moller, C. Hazirbas, and D. Cremers. Learning proximal operators: Using denoising networks for regularizing inverse imaging problems. In *Proceedings of the IEEE International Conference on Computer Vision*, pages 1781–1790, 2017.
- [36] I. Moore, B. Dragoset, T. Ommundsen, D. Wilson, C. Ward, and D. Eke. Simultaneous source separation using dithered sources. *SEG Technical Program Expanded Abstracts*, 2008.
- [37] Y. Romano, M. Elad, and P. Milanfar. The little engine that could: Regularization by denoising (RED). *SIAM Journal on Imaging Sciences*, 10(4):1804–1844, 2017.
- [38] Ernest Ryu, Jialin Liu, Sicheng Wang, Xiaohan Chen, Zhangyang Wang, and Wotao Yin. Plug-and-play methods provably converge with properly trained denoisers. In *International Conference on Machine Learning*, pages 5546–5557. PMLR, 2019.
- [39] Yousef Saad. *Iterative methods for sparse linear systems*. SIAM, 2003.
- [40] R. E. Sheriff and L.P. Geldart. *Exploration Seismology (2nd ed.)*. Cambridge University Press, 1995.
- [41] A. Siahkoohi, M. Louboutin, and F. J. Herrmann. The importance of transfer learning in seismic modeling and imaging. *Geophysics*, 84(6):A47–A52, 2019.
- [42] J. Sun, S. Slang, T. Elboth, T.L. Greiner, S. McDonald, and L.-J. Gelius. A convolutional neural network approach to deblending seismic data. *Geophysics*, 85(4):WA13–WA26, 2020.
- [43] Y. Sun, J. Liu, and U. Kamilov. Block coordinate regularization by denoising. In *Advances in Neural Information Processing Systems*, pages 380–390, 2019.
- [44] J.-B. Thibault, K.D. Sauer, C.A. Bouman, and J. Hsieh. A three-dimensional statistical approach to improved image quality for multislice helical ct.
- [45] T. Tirer and R. Giryes. Image restoration by iterative denoising and backward projections. *IEEE Transactions on Image Processing*, 28(3).
- [46] T. Tirer and R. Giryes. Super-resolution via image-adapted de-noising CNNs: Incorporating external and internal learning. *IEEE Signal Processing Letters*, 26(7).



- [47] S.V Venkatakrishnan, C.A. Bouman, and B. Wohlberg. Plug-and-play priors for model based reconstruction. *2013 IEEE Global Conference on Signal and Information Processing*, 2013.
- [48] S. Wang, W. Hu, P. Yuan, X. Wu, Q. Zhang, P. Nadukandi, G.O. Botero, and J. Chen. Seismic deblending by self-supervised deep learning with a blind-trace network. *SEG/AAPG/SEPM First International Meeting for Applied Geoscience & Energy*, 2021.
- [49] Xiajian Xu, Yu Sun, Jiaming Liu, Brendt Wohlberg, and Ulugbek S. Kamilov. Provable convergence of plug-and-play priors with mme denoisers. *IEEE Signal Processing Letters*, pages 1280–1284, 2020.
- [50] Siwei Yu and Jianwei Ma. Deep learning for geophysics: Current and future trends. *Reviews of Geophysics*, 59(3):e2021RG000742, 2021.
- [51] K. Zhang, Y. Li, W. Zuo, L. Zhang, L. van Gool, and R. Timofte. Plug-and-play image restoration with deep denoiser prior. In *IEEE TPAMI*, 2021.
- [52] K. Zhang, W. Zuo, Y. Chen, D. Meng, and L. Zhang. Beyond a Gaussian denoiser: Residual learning of deep CNN for image denoising. *IEEE Transactions on Image Processing*, pages 3142–3155, 2017.
- [53] K. Zhang, W. Zuo, S. Gu, and L. Zhang. Learning deep cnn denoiser prior for image restoration. In *IEEE Conference on Computer Vision and Pattern Recognition*, pages 3929–3938, 2017.
- [54] H. Zhou, W. Mao, D. Zhang, Q. Ge, and H. Wang. Deblending of simultaneous source with rank-reduction and thresholding constraints. *79th EAGE Conference and Exhibition 2017*, 2017(1):1–5, 2017.
- [55] Y. Zhou, W. Chen, and J. Gao. Separation of seismic blended data by sparse inversion over dictionary learning. *Journal of Applied Geophysics*, 106:146–153, 2014.
- [56] Y. Zhou, J. Gao, W. Chen, and P. Frossard. Seismic simultaneous source separation via patchwise sparse representation. *IEEE Transactions on Geoscience and Remote Sensing*, 54(9):5271–5284, 2016.
- [57] S. Zu, J. Cao, S. Qu, and Y. Chen. Iterative deblending for simultaneous source data using the deep neural network. *Geophysics*, 85(2):V131–V141, 2020.
- [58] S. Zu, H. Zhou, R. Wu, W. Mao, and Y. Chen. Hybrid-sparsity constrained dictionary learning for iterative deblending of extremely noisy simultaneous-source data. *IEEE Transactions on Geoscience and Remote Sensing*, 57(4):2249–2262, 2018.

## A Denoiser progression over iterations

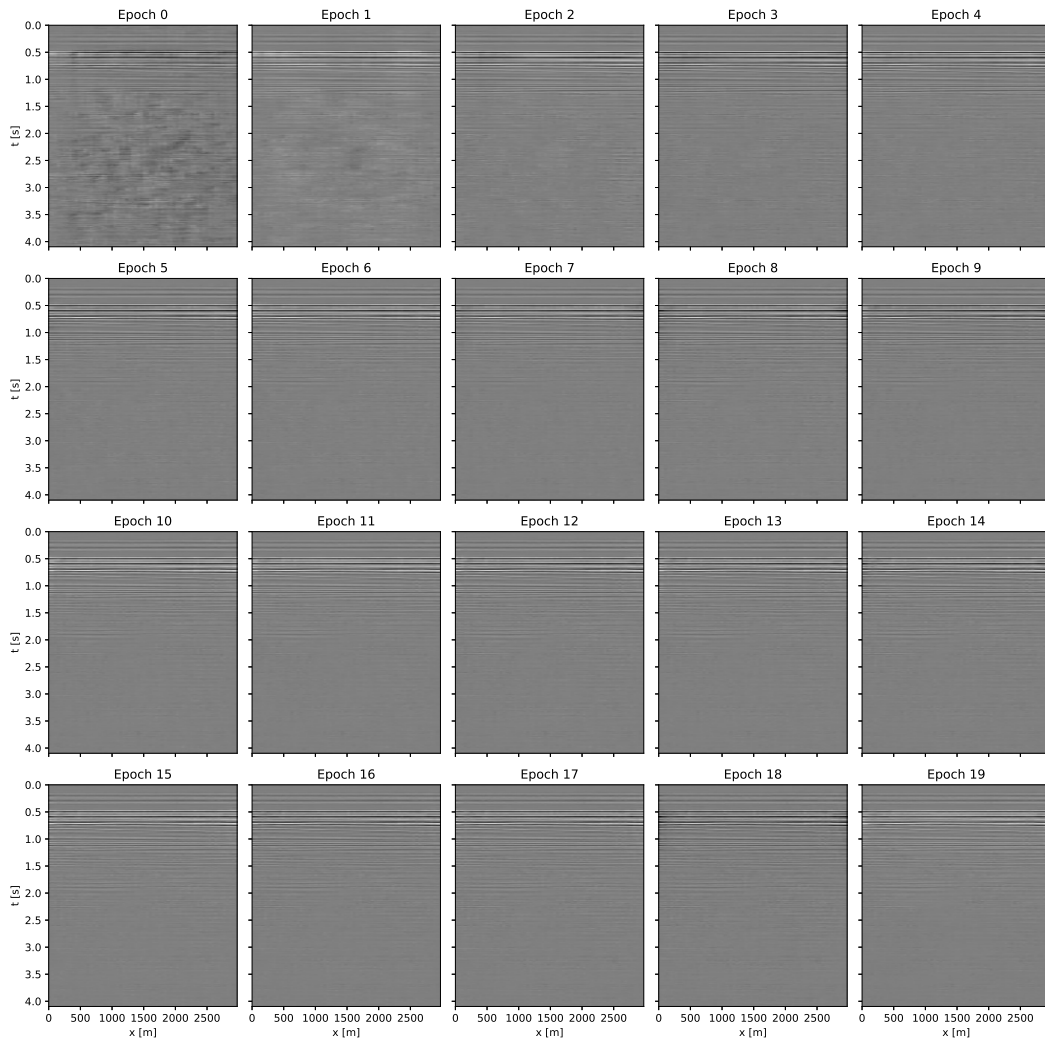


Figure 12: Progression of the denoiser for outer iteration 1.

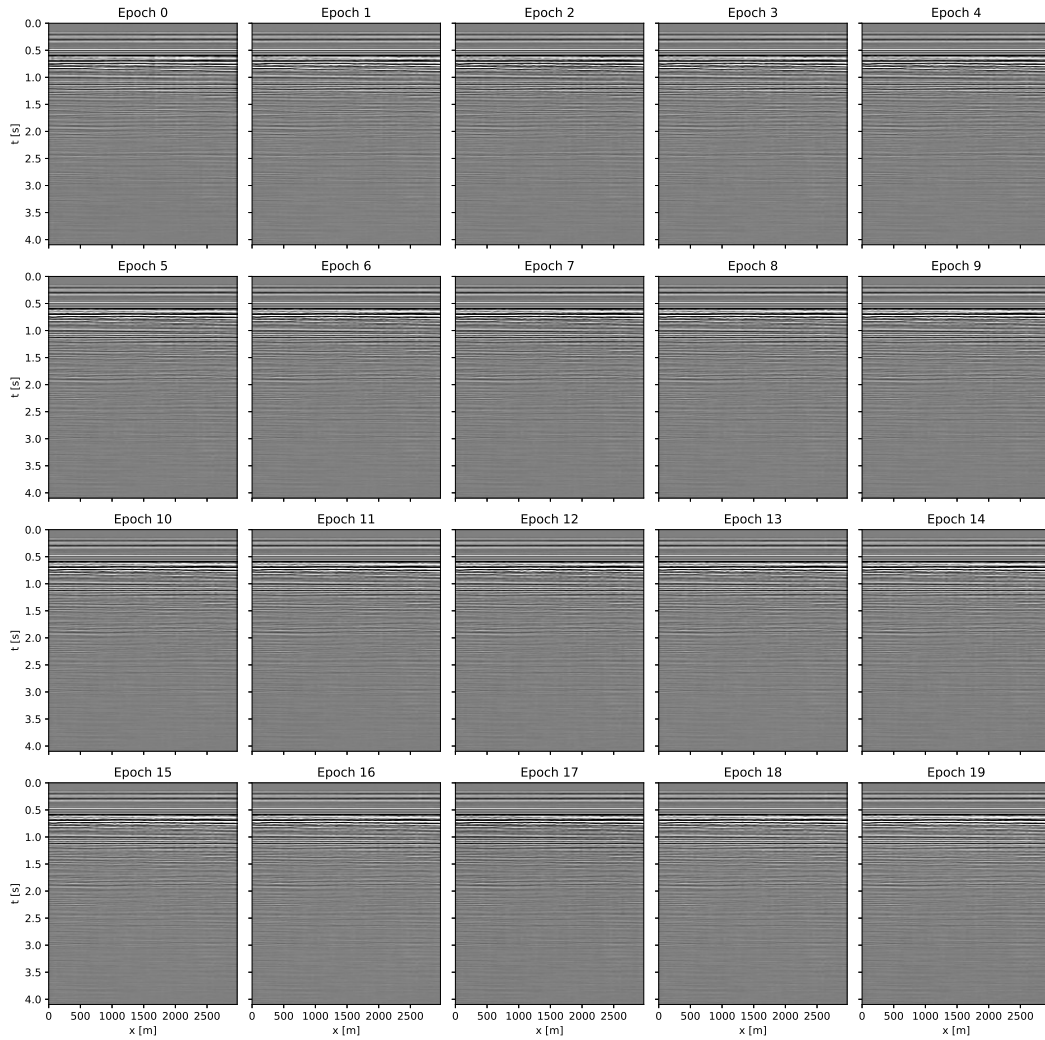


Figure 13: Progression of the denoiser for outer iteration 10.

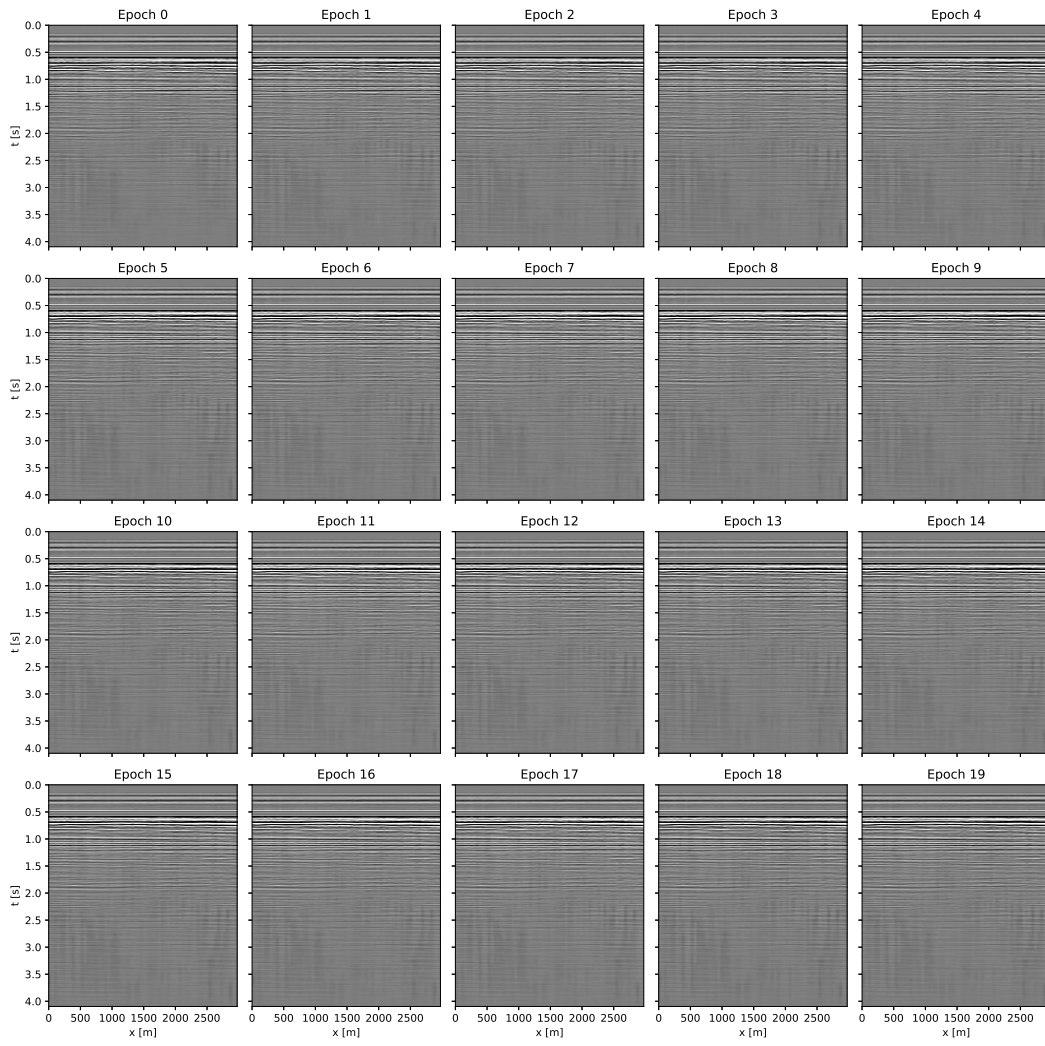


Figure 14: Progression of the denoiser for outer iteration 20.

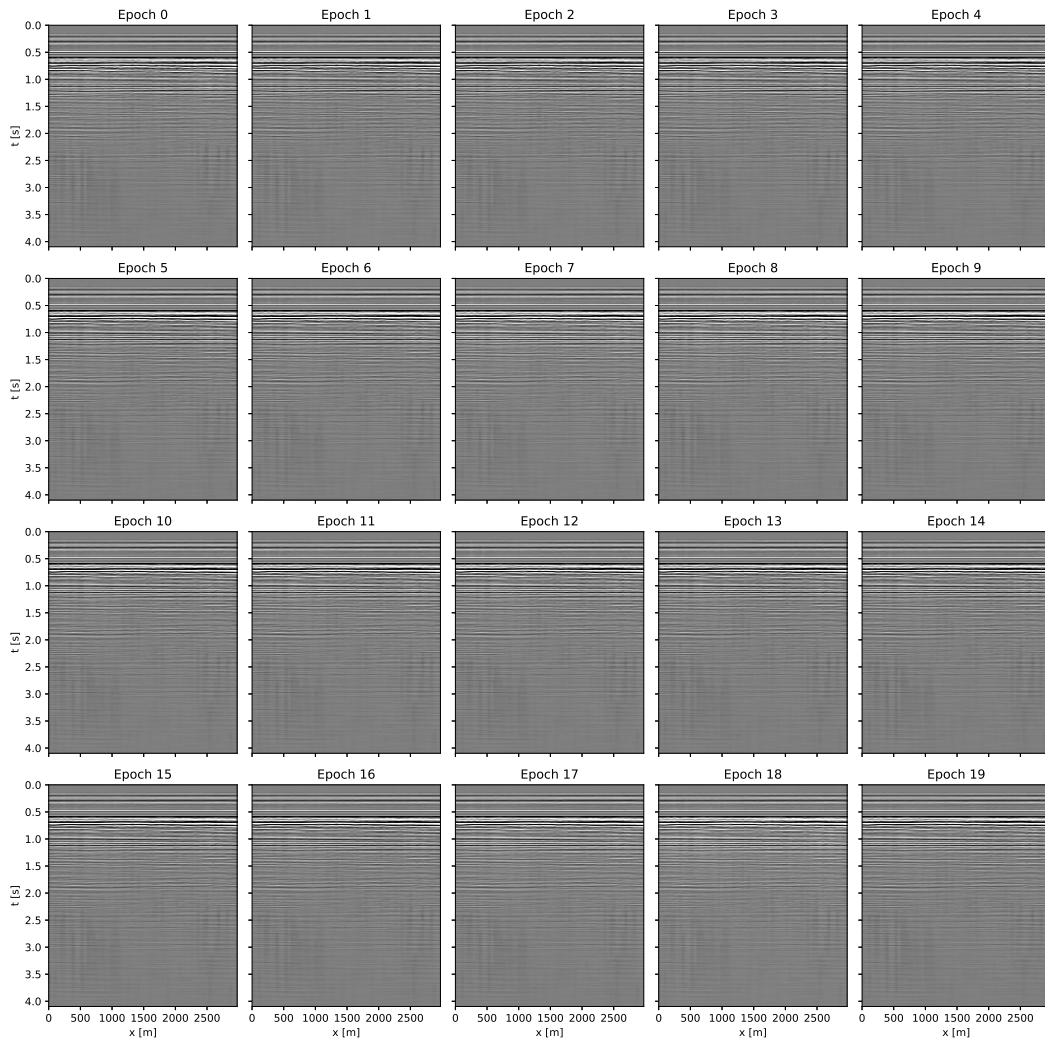


Figure 15: Progression of the denoiser for outer iteration 30.